Deep immunophenotypic dissection and clinical impact of T cells in the follicular lymphoma microenvironment

Sary El Daker,[1] David Qualls,[2] Andriy Derkach,[3] Samida Beqaj,[1] Leonardo Boiocchi,[1] Venkatraman Seshan,[3] Jeeyeon Baik,[1] Menglei Zhu,[1] Gilles Salles,[2] Ahmet Dogan,[1] Mikhail Roshal[1] and Pallavi Galera[1]

[1]Hematopathology Service, Department of Pathology and Laboratory Medicine (a member of the imCORE Network); [2]Lymphoma Service, Department of Medicine and [3]Department of Epidemiology and Biostatistics, Memorial Sloan Kettering Cancer Center, New York, NY, USA

Correspondence: P. Galera
GaleraP@mskcc.org

Received: August 2, 2024.
Accepted: January 20, 2025.
Early view: February 6, 2025.

https://doi.org/10.3324/haematol.2024.286383

Deep immunophenotypic dissection and clinical impact of T-cells in the follicular lymphoma microenvironment

Running title: Follicular Lymphoma T-cell Microenvironment

Sary El Daker[1], David Qualls[2], Andriy Derkach[3], Samida Beqaj[1], Leonardo Boiocchi[1], Venkatraman Seshan[3], Jeeyeon Baik[1], Menglei Zhu[1], Gilles Salles[2], Ahmet Dogan[1], Mikhail Roshal[1], Pallavi Galera[1].

[1] Hematopathology Service, Department of Pathology and Laboratory Medicine*

[2] Lymphoma Service, Department of Medicine

[3] Department of Epidemiology and Biostatistics

* A member of the imCORE Network

Memorial Sloan Kettering Cancer Center, New York, NY, USA

Supplementary Methods

Cell processing/staining and acquisition

Flow cytometry staining was performed using standard protocols for nuclear markers provided by Invitrogen (FoxP3/Transcription factor staining buffer set). Tissue samples were placed into a 70mm cell strainer on top of a conical 50mL tube containing RPMI-1640, 10% NBCS and penicillin/streptomycin preparation. The thumb press of a 1mL syringe plunger was used to crush the sample and dissociate the cells. The strainer was washed periodically until all the tissue was dissociated. The strained cell suspension was washed twice, and cells were finally counted and resuspended at the designed concentration. Tissue suspensions were stained with a cocktail of surface antibodies for 15 minutes at room temperature. Cells were washed with PBA buffer, and the cell pellets were resuspended in Fix/Perm working solution. After 15 minutes of incubation at room temperature protected from light, cells were washed with Perm buffer 1X, and the pellet was resuspended in 200 microliters of a cocktail containing antibodies directed towards intracellular antigens (FoxP3, Tbet, Ki67, and CTLA4). Cells were incubated for 30 min at room temperature, protected from light. After incubation, cells were washed twice in Perm buffer and resuspended in 100 microliters of PBA.

Multiplex immunofluorescence

Tissue sections were prepared for a 6-plex immunofluorescence assay targeting CD20, CD4, FoxP3, PD-1 and BCL-6 antigens (Table S3). Staining was performed on the Leica BOND RX automatic staining platform. Antigen retrieval was performed using the Epitope Retrieval Solution 2, incubated for 20 mins on the BOND. The sections were then incubated sequentially with the primary antibodies each diluted to varying concentrations after validation on control tissue. Each antibody was followed by the secondary polymer SuperBoost™ Goat anti-Mouse Poly HRP or SuperBoost™ Goat anti-Rabbit Poly HRP (ThermoFisher) and its corresponding fluorophore from Akoya Bioscience's Opal 6-Plex Detection Kit. After staining is complete, the slides were counterstained with DAPI and then mounted with ProLong Gold antifade reagent (ThermoFisher). The slides were imaged using the Vectra Polaris PhenoImager (Akoya Bioscience), and then analyzed using the image analysis platform HALO.

Statistical analysis

The proportions of T-cell populations were tested across the cohorts using the Kruskal-Wallis test. Pairwise comparison was performed when the Kruskal-Wallis test was significant and a Bonferroni correction was applied. The cell counts obtained from the cell processing step for the 19 T-cell subsets were normalized to express the counts as number per 1000 cells to account for varying total cell counts across samples.

For the unsupervised clustering of the samples the normalized data were further categorized into quartiles of the distribution of normalized cell counts across samples. This categorization accounts for the difference in median cell counts by immune cell type as well as the skewness in the distributions. The cell counts across the three classes were compared using Kruskal-Wallis test. Closed testing procedure with Bonferroni correction was used for pairwise comparisons for immune cell types for which the null hypothesis of same distributions for all three groups was rejected.

Similarly, associations between clinical variables and percentages of immune suppressive populations were evaluated by using Kruskal-Wallis test. Selection cut-off thresholds for these continuous biomarkers for optimal association with time to start of a treatment was conducted using maximally selected rank statistics.[1] Lastly associations between clusters and time to event outcomes were evaluated by log-rank test.

Supplementary Figure 1:

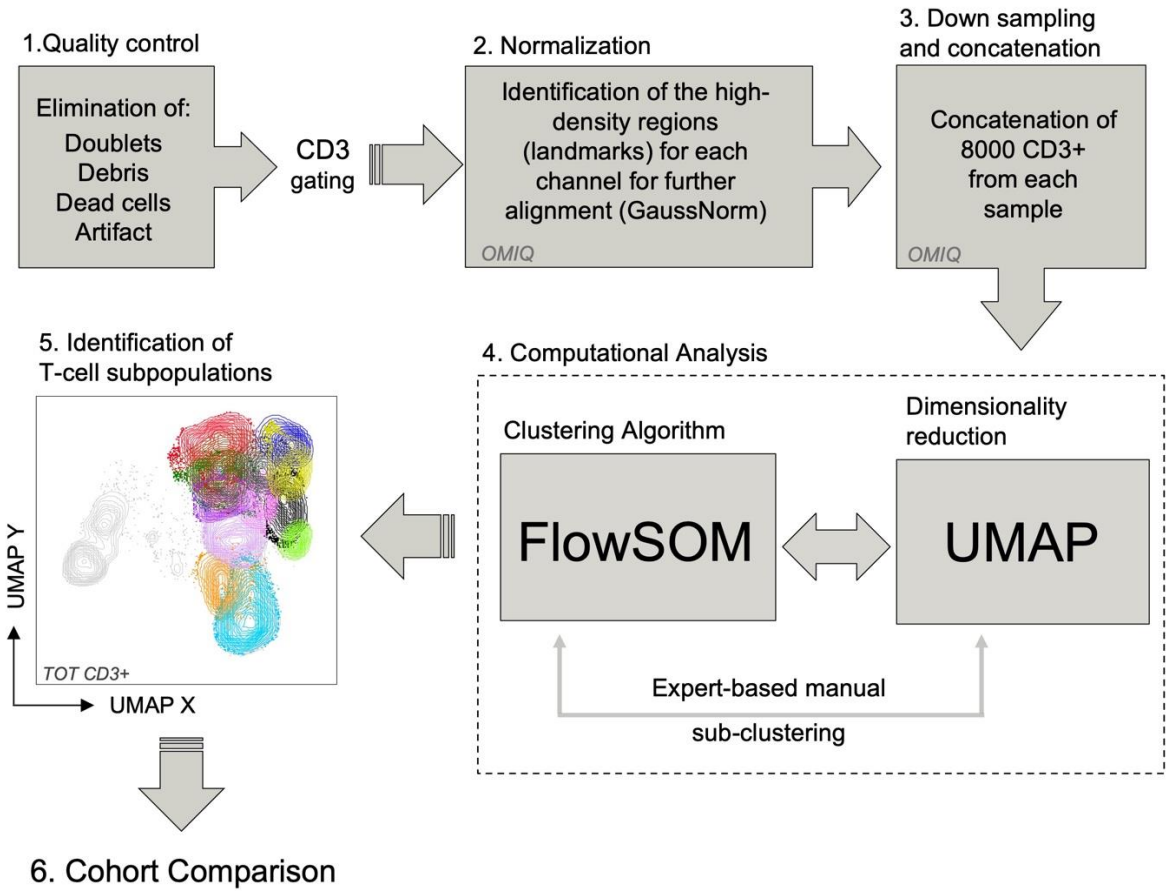

Figure S1. Overview of the analytical pipeline used to analyze single-cell suspensions derived from reactive and B-cell lymphoma isolates. Research Panel I was been analyzed using the following pipeline: scatter parameters were used to remove doublets, debris, dead cells and artifacts from every single file. T cells were identified using CD3 antibody and scatter parameters and used as input for the analytical pipeline. To minimize technical variation in sample acquisition over time we used an R-based algorithm (GaussNorm). 8000 CD3+ events from each sample were concatenated and the file generated (containing both reactive follicular hyperplasia and follicular lymphoma specimens) was used to identify the T-cell subpopulations by combining a dimensionality reduction technique (UMAP) with an unsupervised clustering algorithm (FlowSOM). Expert-based manual sub-clustering was performed to refine phenotypes that showed excessive heterogeneity.

Supplementary Figure 2:

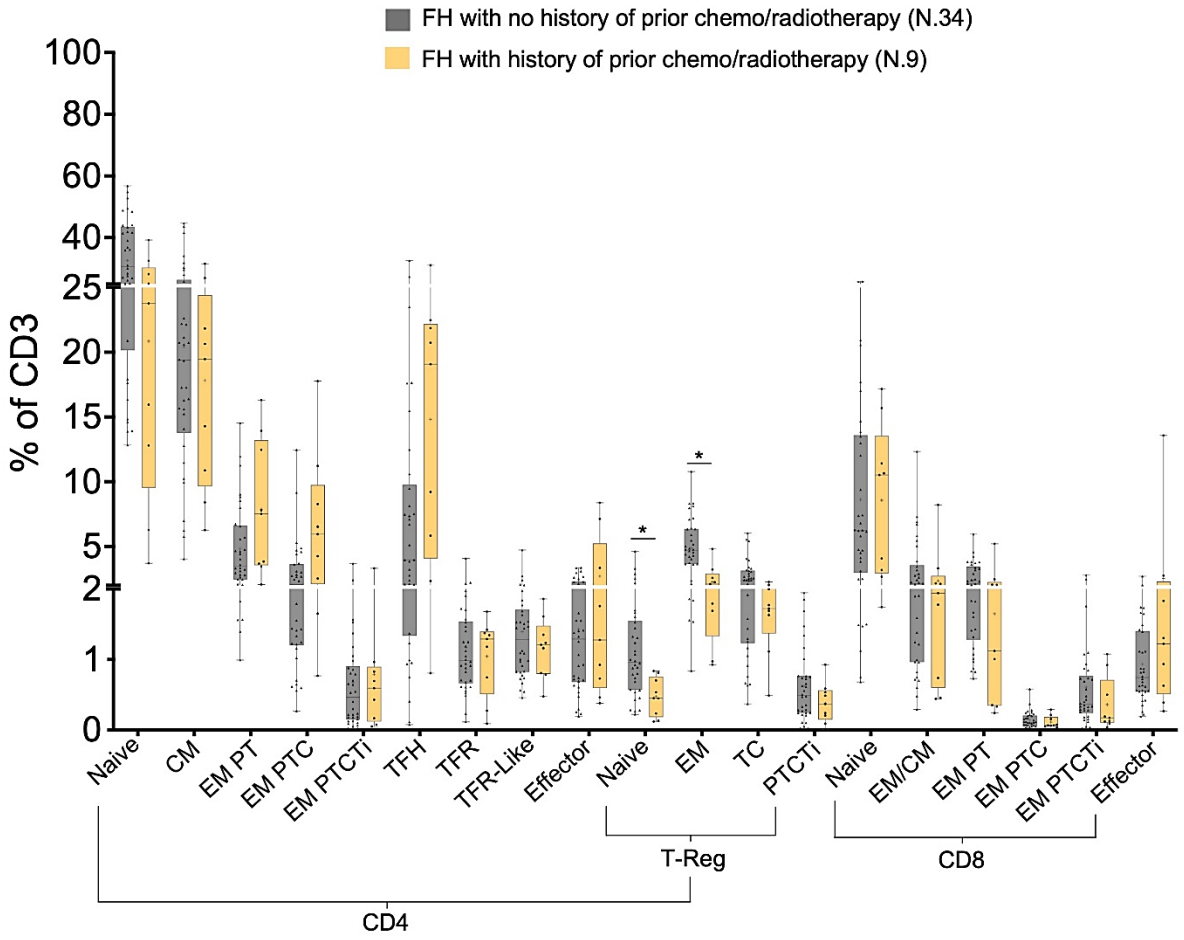

Figure S2. Distribution of various T-cell subsets in FH cohort comparing patients with no history of prior chemo/radiotherapy and patients with prior therapy.

Supplementary Figure 3:

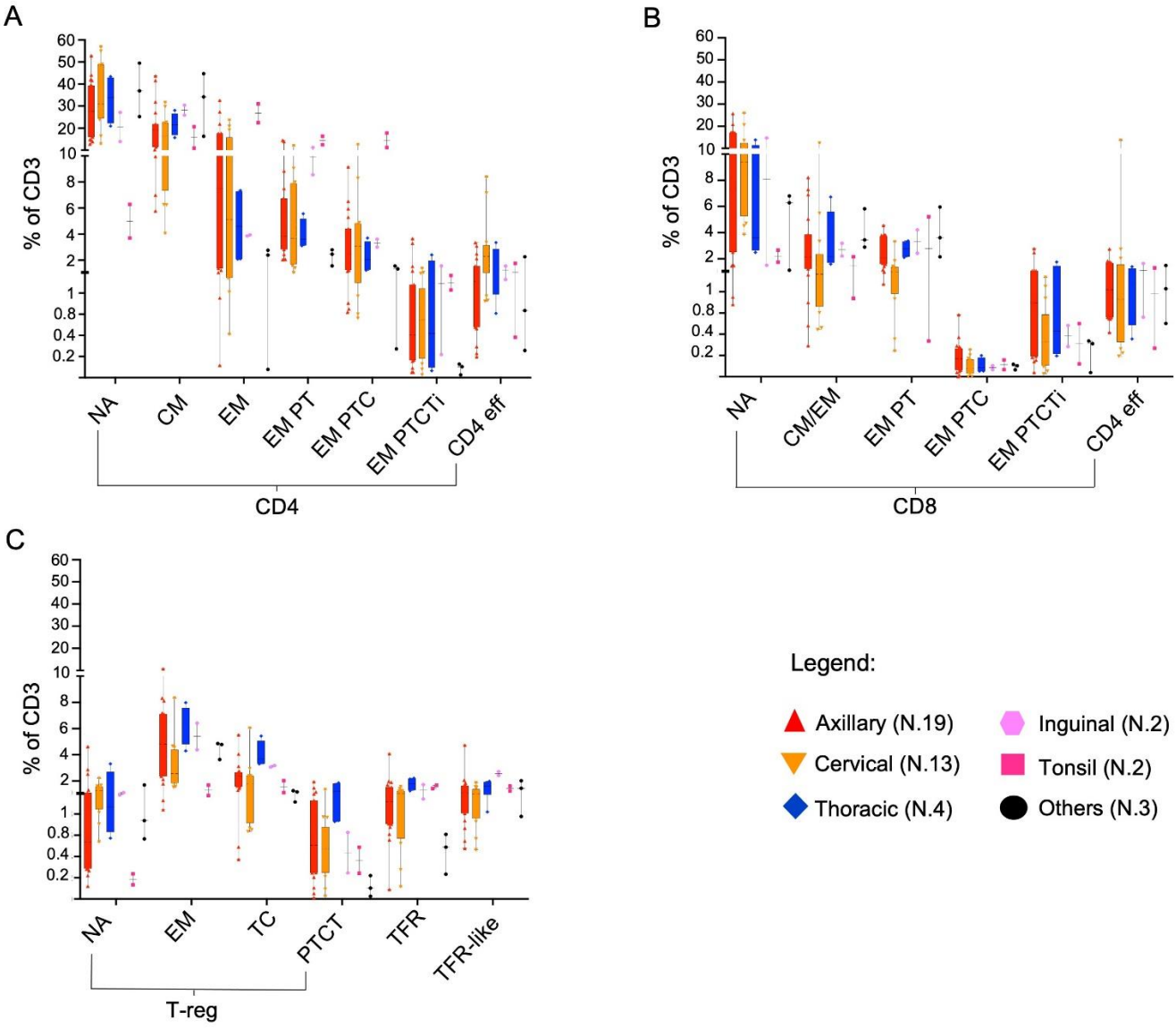

Figure S3. Distribution of various T-cell subsets in FH cohort comparing various anatomical sites of sampling.
(A) CD4+ T-cell subsets. (B) CD8+ T-cell subsets. (C) T-regulatory cells.

Supplementary Figure 4:

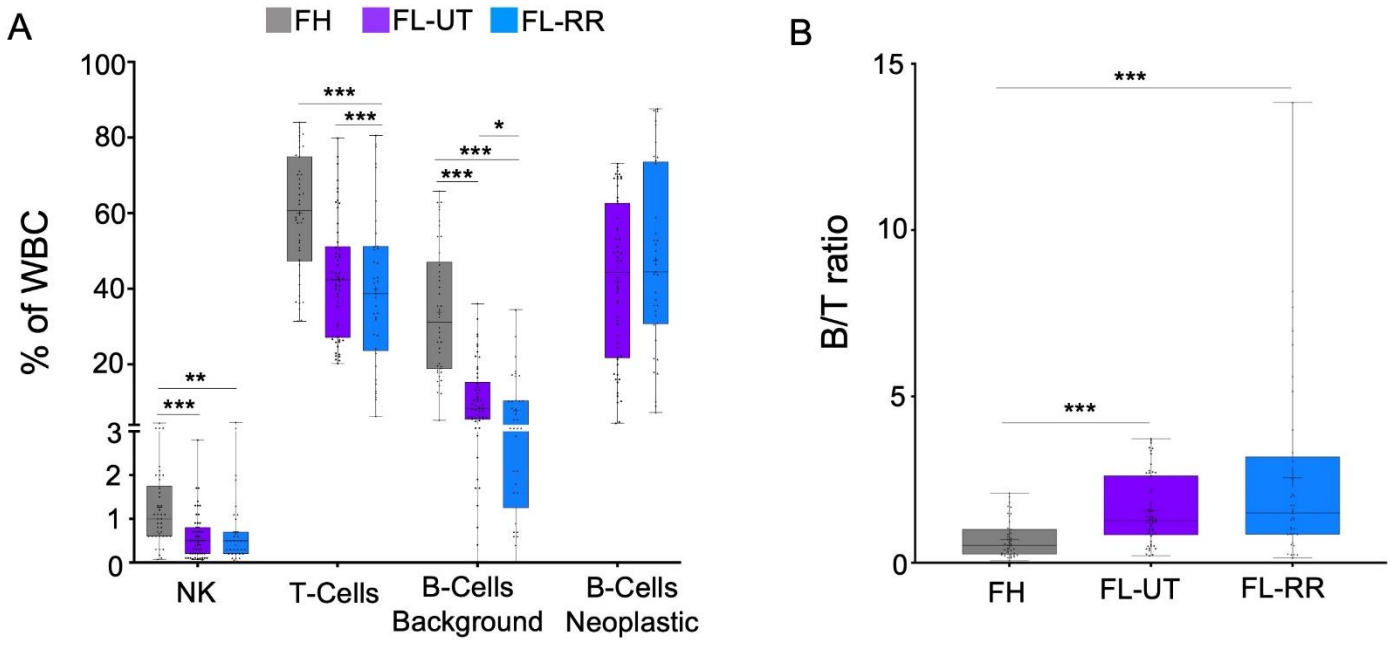

Figure S4. Clinical characterization of reactive (FH) and follicular lymphoma (FL-UT, FL-RR) specimens. (A) Percentage of NK-cells, T-cells, background non-neoplastic B-cells and neoplastic B-cells in FH and FL specimens (FL-UT and FL-RR). (B) B/T ratio in FH and FL specimens. p- value *** ≤ 0.0001 ** ≤ 0.001 *≤ 0.02

Supplementary Figure 5:

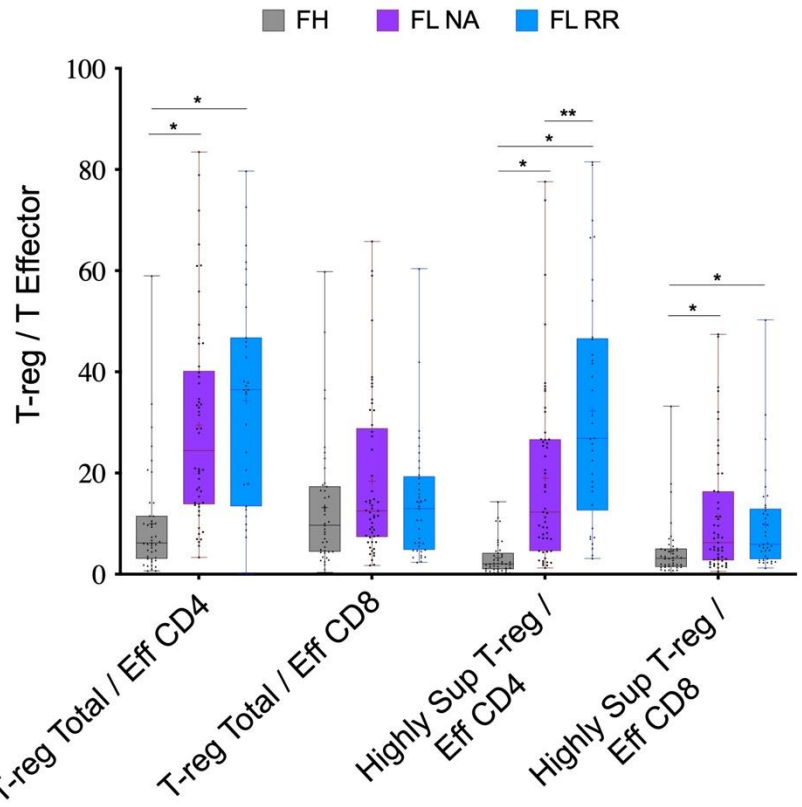

Figure S5. Regulatory T-reg/Effector T cells ratio in reactive (FH) and follicular lymphoma (FL-UT, FL-RR) specimens. Ratio between T-reg Total (T-reg naïve, T-reg EM, T-reg TC and Treg PTCTi), Highly suppressive T-reg (T-reg TC and T-reg PTCTi) and effector CD4 and effector CD8 was calculated. p- value ** ≤ 0.001 *≤ 0.02

Supplementary Figure 6:

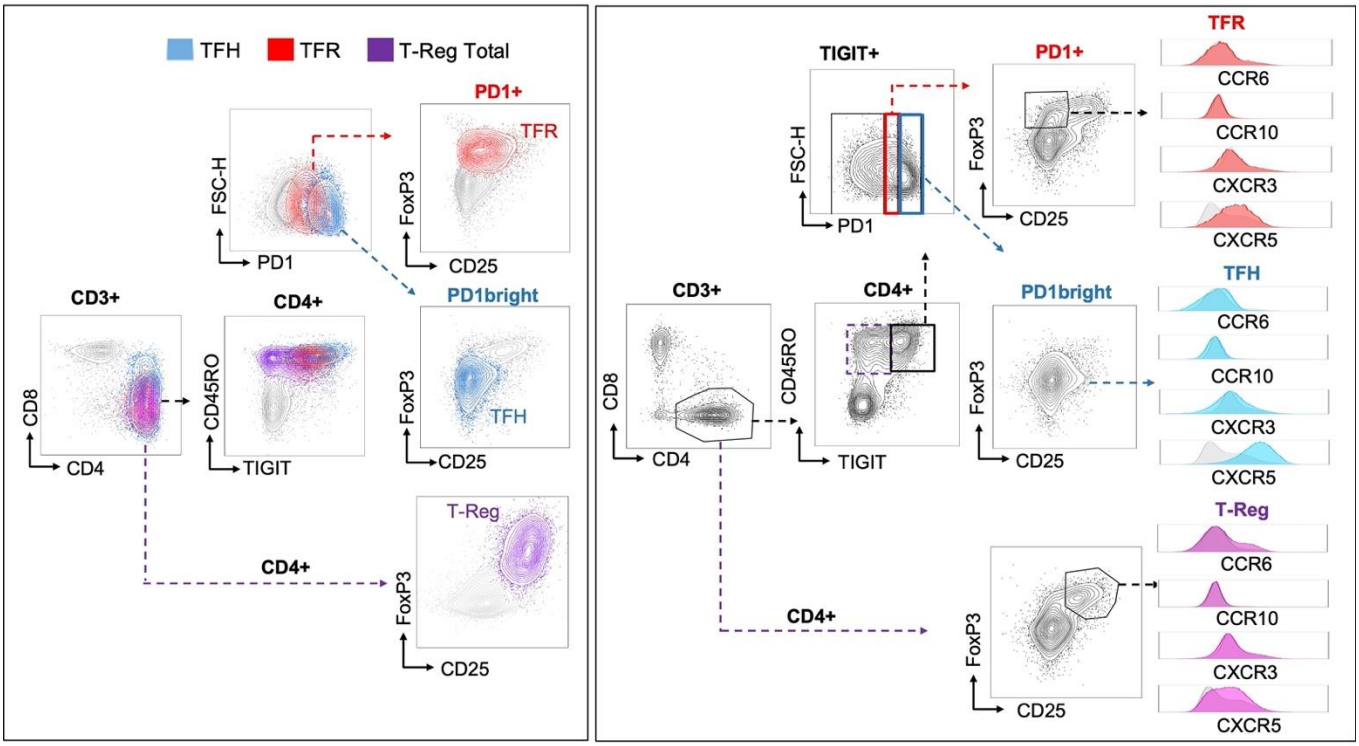

Figure S6. Additional characterization of TFH, TFR and T-regulatory cell (T-reg) populations. We utilized research panel II to further define the phenotype of populations identified by research panel I. Using a manual gating strategy, common markers between the research panels and the phenotype identified through computational analysis with research panel I, were used to identify TFH, TFR and T-Reg subpopulations in research panel II. These populations were further characterized by the expression of the chemokine receptors CCR6, CCR10, CXCR3, and CXCR5.

Supplementary Figure 7:

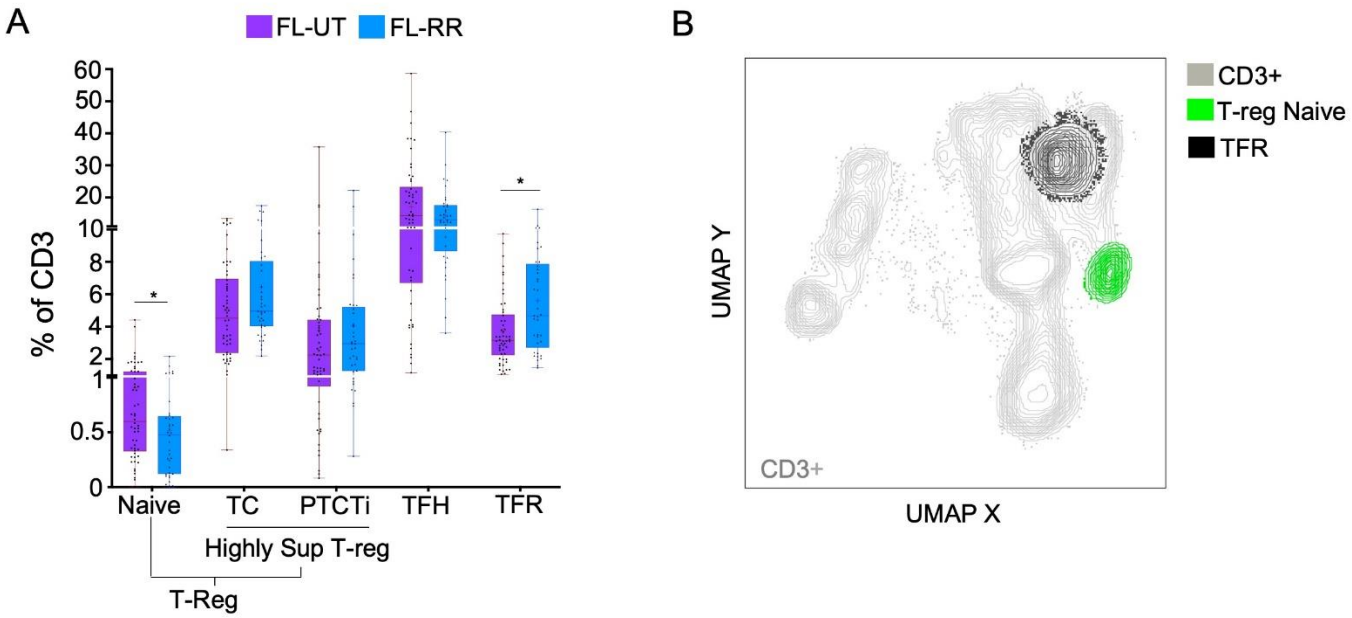

Figure S7. Alterations in FL-RR microenvironment in comparison to FL-UT. (A) Percentage of T-reg naïve, T-reg TC, Treg PTCTi, TFH and TFR in FL-UT and FL-RR. p- value *≤ 0.02. **(B)** Uniform Manifold Approximation and Projection (UMAP) of T-reg naïve and TFR in FL-UT and FL-RR.

Supplementary Figure 8:

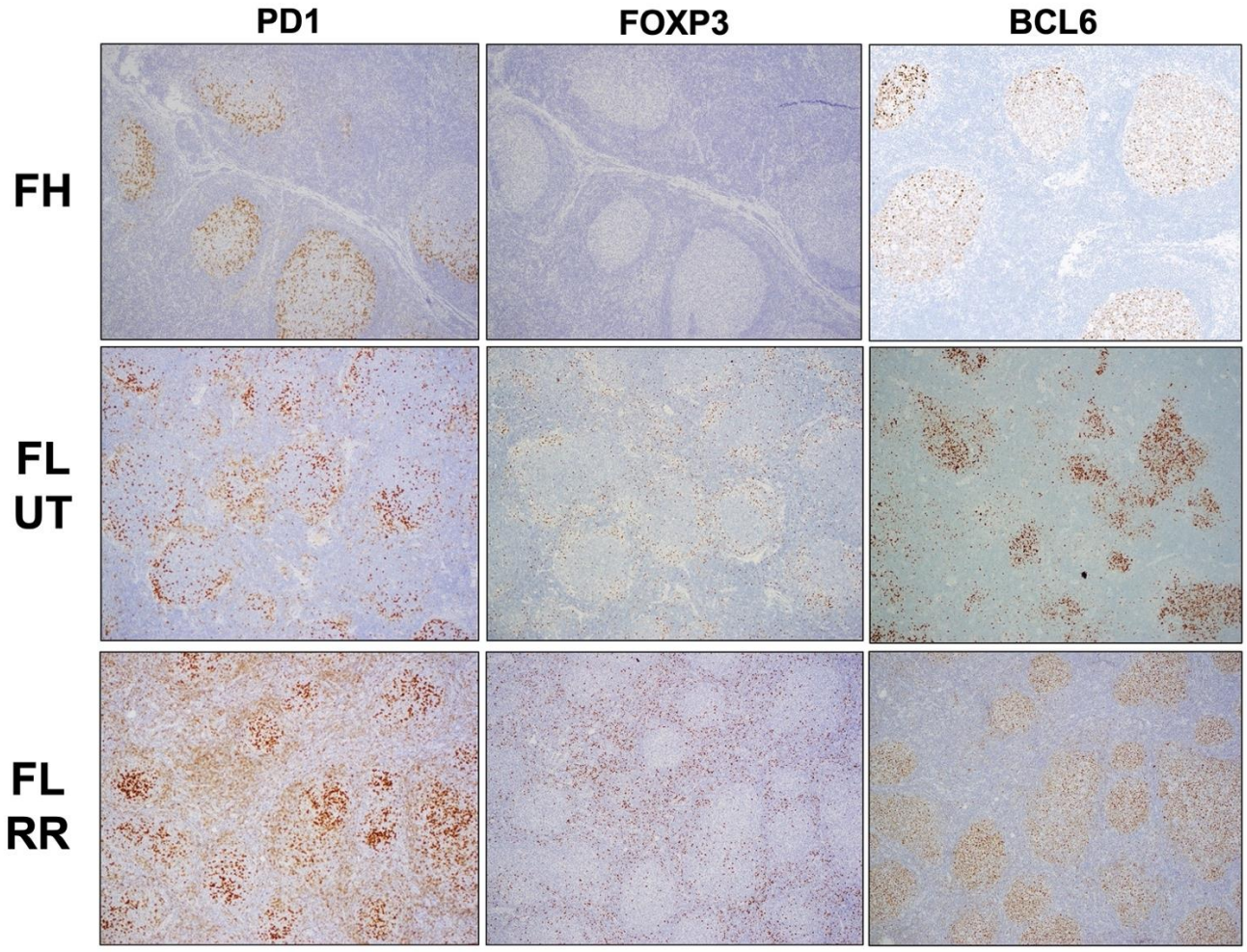

Figure S8. Immunohistochemical staining for PD1, FoxP3 and BCL-6 on reactive follicular hyperplasia (FH) and follicular lymphoma, untreated and relapsed/ refractory (FL-UT and FL-RR) specimens. In the FH specimen, PD1 brightly positive T-follicular helper cells (TFH) cells are present within the germinal centers and are polarized predominantly to the light zone. In the FL specimens, PD1 brightly positive TFH cells are seen within the neoplastic follicles and the dim PD1 positive, FoxP3 positive, BCL6 positive T-follicular regulatory cells (TFR) cells are seen within and surrounding the neoplastic follicles. Both TFH and TFR cells are present in higher density in both the FL specimens (FL-UT and FL-RR) vs FH specimen. TFR cells are present in a significantly higher frequency in FL-RR cases in comparison to both FH and FL-UT.

Supplementary Figure 9:

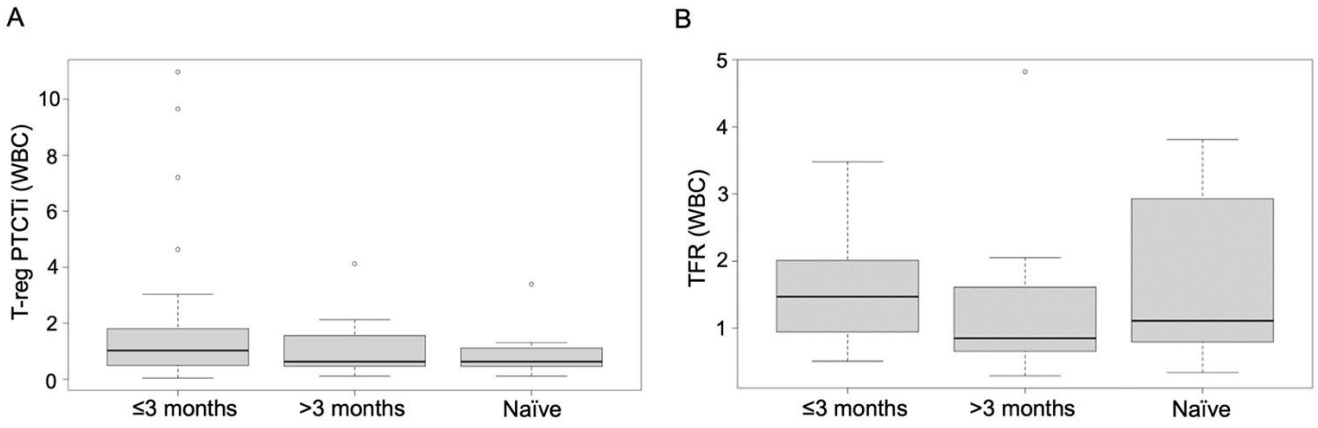

Figure S9. Correlation of T-reg PTCTi and TFR with earlier initiation of the therapy in FL-UT cohort. (A-B) T-reg PTCTi and TFR represented as percent of WBC plotted against time to first treatment (>3 months, <3 months).

Supplementary Figure 10:

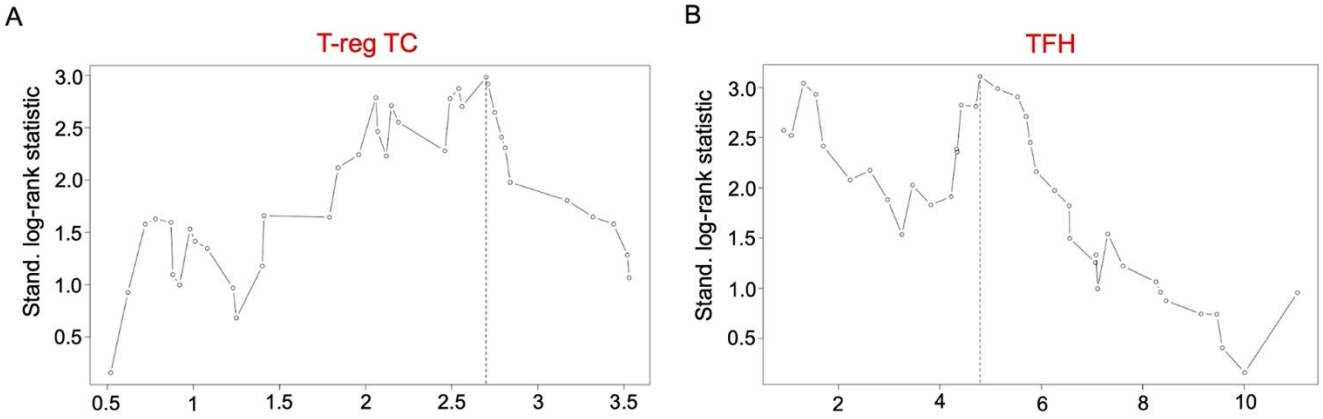

Figure S10. Maximally selected rank statistics on the FL-UT cohort. (A, B) Estimated optimal cutoff points for T-reg TC and TFH percentages are 2.7% and 4.79% of WBC, respectively.

Supplementary Figure 11:

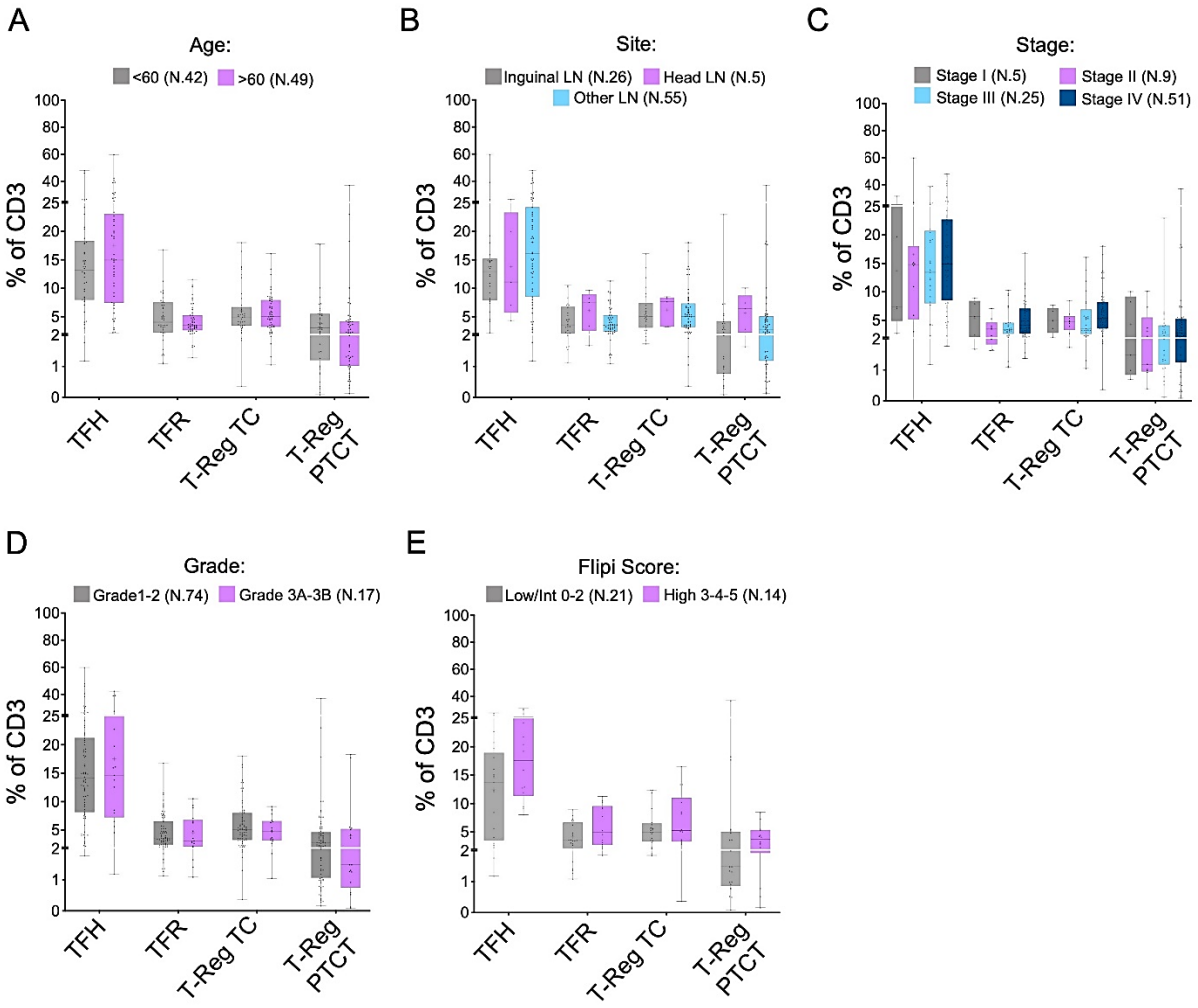

Figure S11. Distribution of immunosuppressive populations (T-reg TC, T-reg PTCTi and TFR) and TFH among various clinicopathological settings in both FL cohorts. (A) Age. (B) Site. (C) Stage. (D) Grade. (E) FLIPI score.

Supplementary Figure 12:

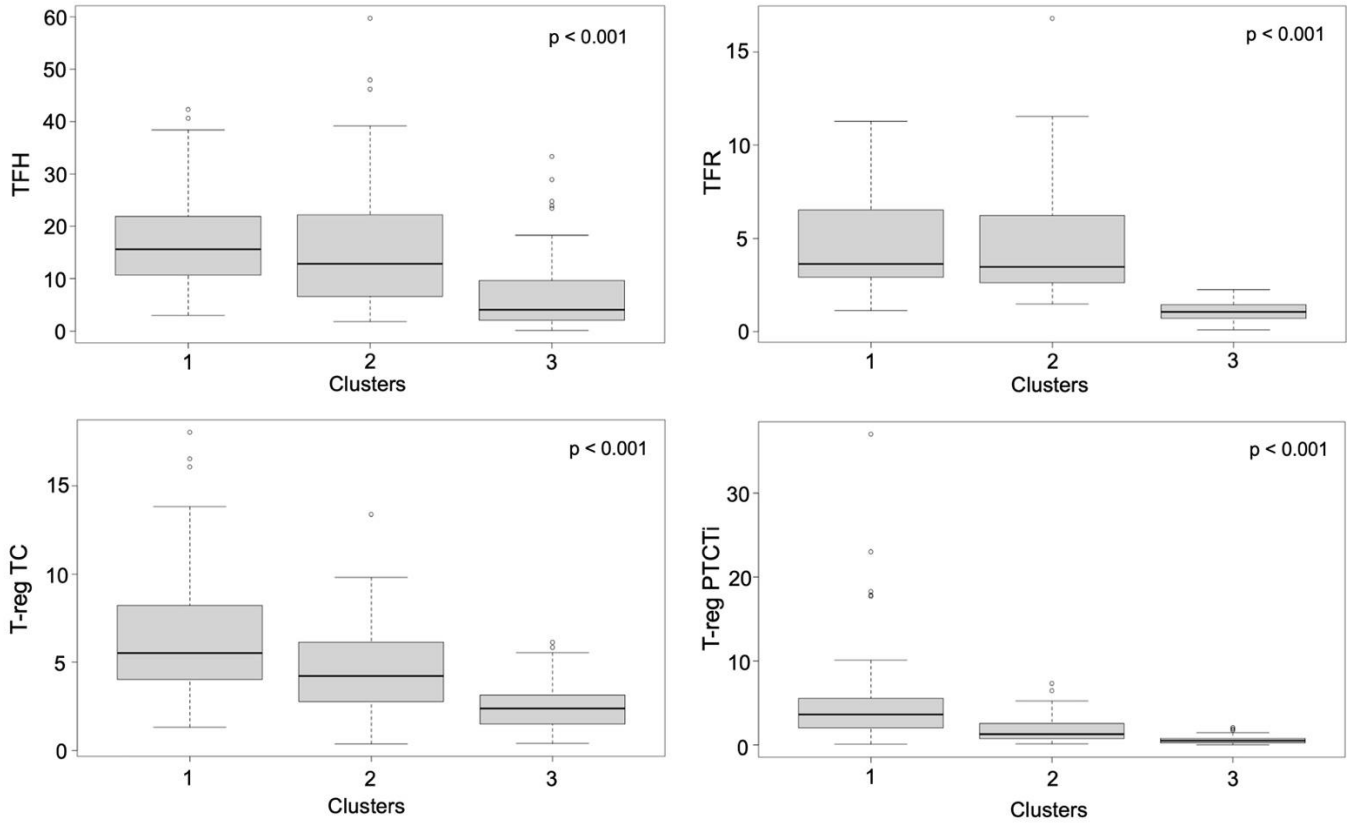

Figure S12. Distribution of T-cell subsets as percentage of WBCs in the 3 clusters identified by unsupervised hierarchical clustering that show statistical difference between the 3 clusters.

Supplementary Figure 13:

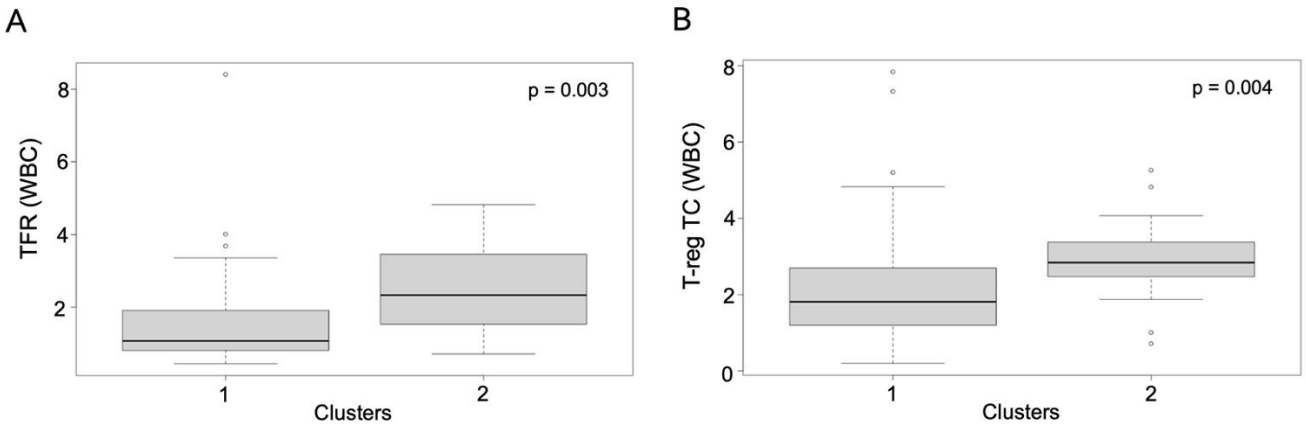

Figure S13. Distribution of T-cell subsets as percentage of WBCs in the clusters 1 and 2 (enriched in FL cases) that show statistical difference between the 2 clusters. (A) TFR. (B) T-reg TC.

Supplementary Figure 14:

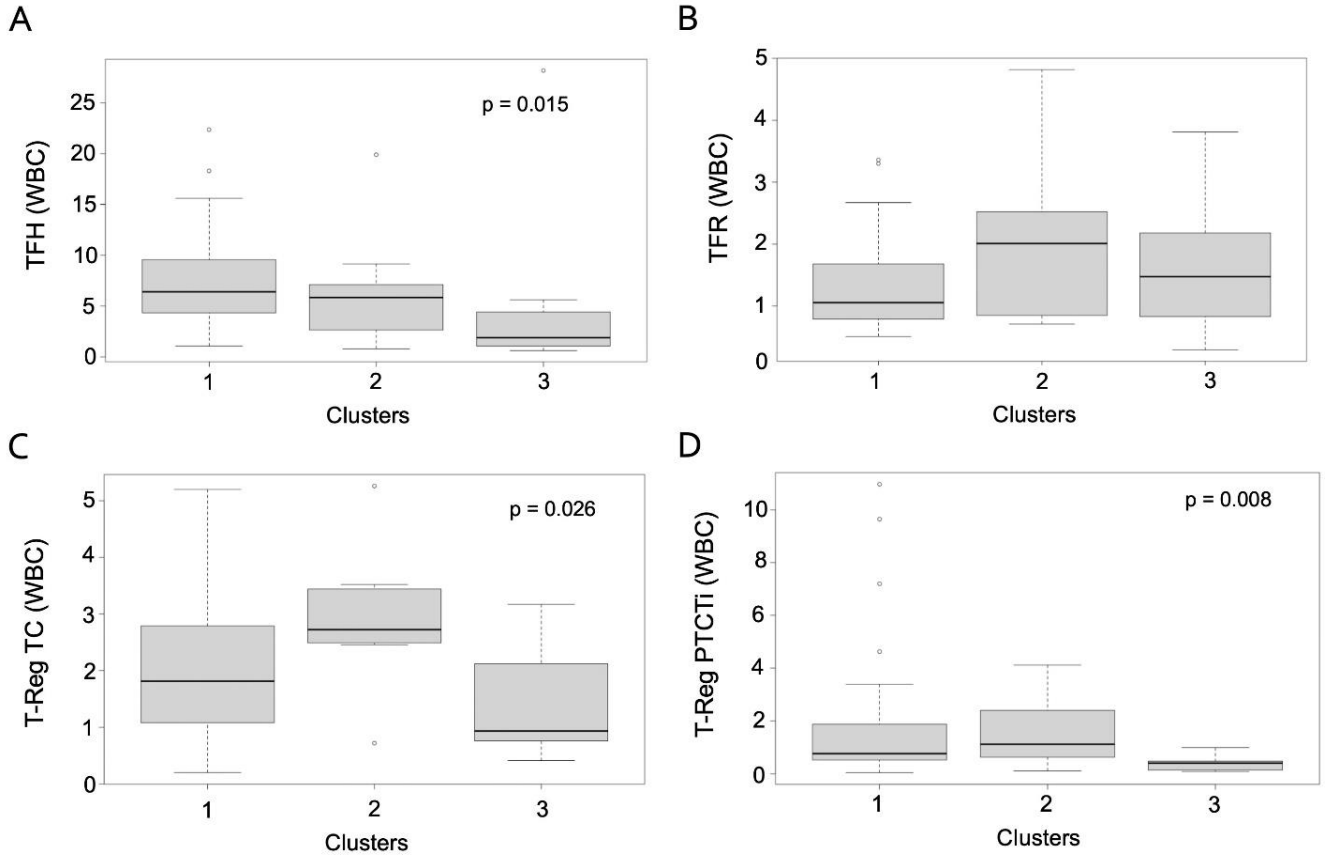

Figure S14: Distribution of T-cell subsets as percentage of WBCs in "FH-like FL" cases (10 FL-UT cases) in cluster 3 in comparison to other FL-UT cases present in clusters 1 and 2. (A) TFH. (B) TFR. (C) T-reg TC. (D) T-reg PTCTi.

Supplementary Figure 15:

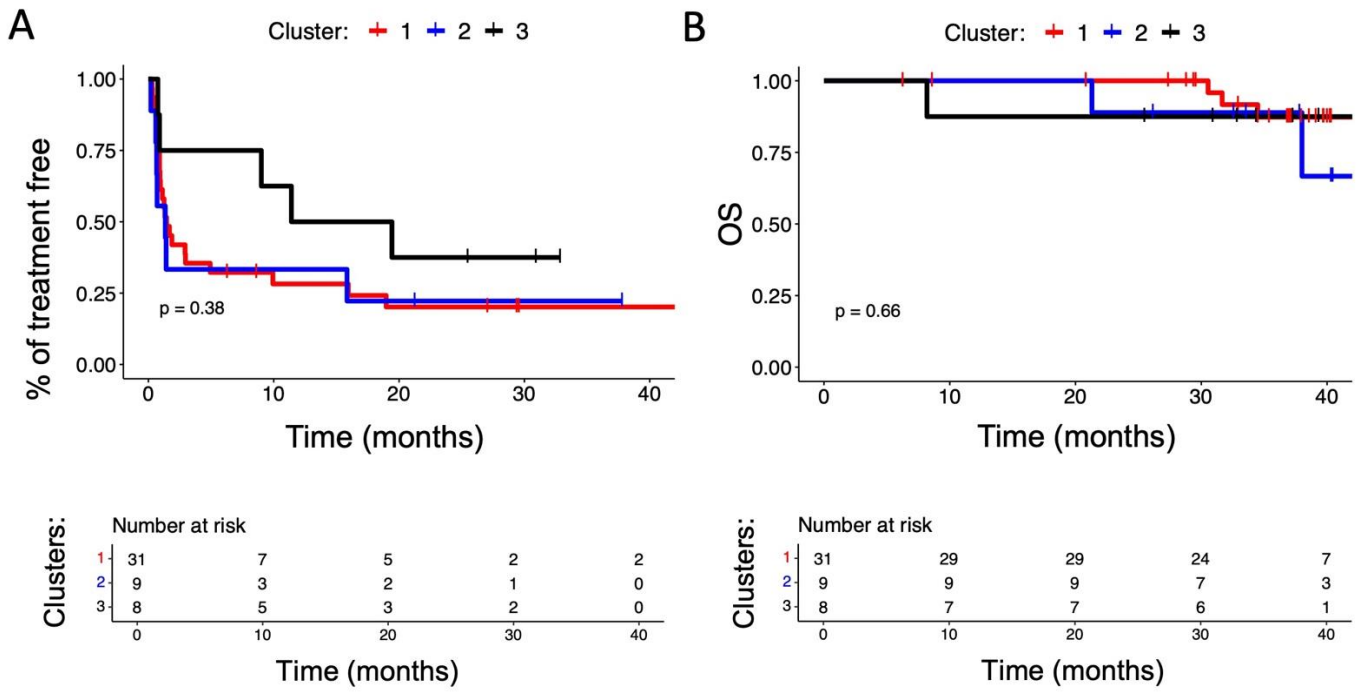

Figure S15. Kaplan Meier curve comparing FL-UT cases in cluster 1, cluster 2 and cluster 3 ("FH-like FL" cases). (A) Kaplan Meier curve illustrating time to first treatment of the FL-UT cases in cluster 1, cluster 2 and cluster 3 ("FH-like FL" cases) depicted in red, blue, and black curves, respectively. (B) Kaplan Meier curve illustrating overall survival of the FL-UT cases in cluster 1, cluster 2 and cluster 3 ("FH-like FL" cases) depicted in red, blue, and black curves, respectively.

Reference:

1. Hothorn T, Lausen B. On the exact distribution of maximally selected rank statistics. *Computational Statistics & Data Analysis*. 2003/06/28/ 2003;43(2):121-137.

Supplementary Tables

For Supplementary Tables from Table S1 to Table S9 please see separte Excel file